**Working Draft2_3006**

# Single-Exciton Amplified Spontaneous Emission in Thin Films of $CsPbX_3$ (X=Br, I) Perovskite Nanocrystals

Juan Navarro-Arenas,[1] Isaac Suárez,[1,2*] Vladimir S. Chirvony,[1] Andrés F. Gualdrón-Reyes,[3] Iván Mora-Seró,[3] Juan Martínez-Pastor[1*]

*[1]Instituto de Ciencia de Materiales (ICMUV), Universidad de Valencia, C/ Catedrático José Beltrán, 2, 46980 Paterna, Spain;*
*[2]School of Telecommunications Engineering, Electronics Area, Camino del Molino s/n 28942 Fuenlabrada, Spain;[3]Institute of Advanced Materials (INAM), Universitat Jaume I, Castelló 12006, Spain*

## Abstract

During the last four years, $CsPbX_3$ perovskite nanocrystals (PNC) have emerged as an excellent material for stimulated emission purposes, with even more prospective properties than conventional colloidal quantum dots. However, although the results under femtosecond excitation undoubtedly demonstrate potential performances, the achievement of more ambitious targets, such as stimulated emission under cw optical or electrical excitation, requires a better understanding of the physical and optical mechanisms responsible for the generation of the optical gain. In this publication, we establish intrinsic mechanisms underlaying the generation of amplified spontaneous emission (ASE) in PNCs with three different bandgaps ($CsPbBr_3$, $CsPbI_3$, and $CsPbBr_{1.5}I_{1.5}$). For this purpose, optical gain is characterized at cryogenic temperatures in order to avoid the influence of non-radiative channels. In particular, our experimental results provide physical evidences that single excitons are the dominant species in the ASE generation. Moreover, the particular shape of ASE spectra is well reproduced by the model that takes into account the reabsorption effects and the inhomogeneous broadening of the PL band. These results are a new milestone towards the full understanding of light generation in PNCs, and with the development of competitive active optoelectronic devices.

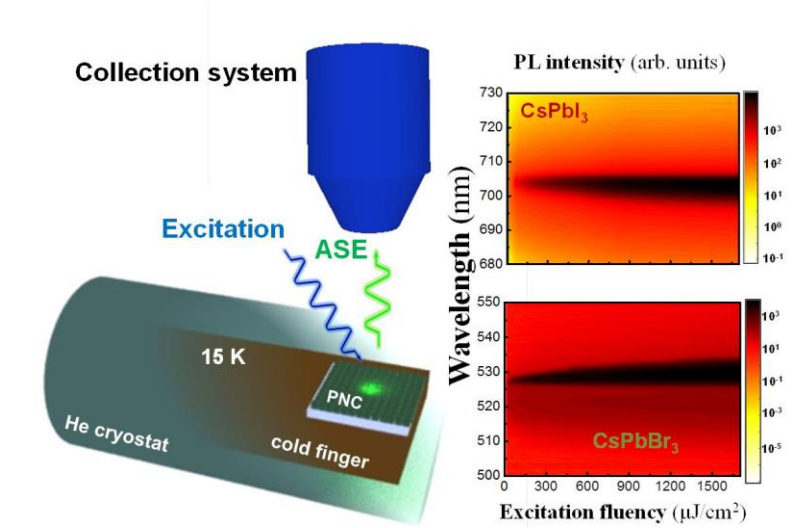


TOC ABSTRACT

## Introduction

During the last years, colloidal quantum dots (CQD) have been extensively studied as a cheap alternative to epitaxial III-V semiconductors for optical gain purposes.[1,2] Since the first demonstration of the amplified spontaneous emission (ASE) in 2000,[3] a significant progress has been achieved[2] including the demonstration of lasing under continuous wave operation in 2017,[4] and more recently, under electrical pumping in 2018.[5] In particular, several important milestones have been overcome by means of thorough study of optical gain mechanisms in optically excited CQDs: (i) resolving the problem of Auger recombination by employing femtosecond (fs) excitation and densely packed QD films;[6] (ii) understanding of the impossibility to obtain gain in neutral (uncharged) core-only QDs within single exciton regime;[7] (iii) increasing absorption cross-sections using large-volume nanostructures;[8] (iv) the introduction of permanent charges for reducing the gain threshold due to partial blocking of ground state absorption.[9]

On the other hand, metal halide perovskite nanocrystals (PNCs) have recently emerged as a new class of colloidal nanocrystals with improved performances for active devices.[10] Compared with conventional CQDs, PNCs demonstrate larger absorption cross sections,[11] quantum yield of emission higher than 90 %,[12] and higher packing density allowed by the particular nanocube geometry.[10] In fact, PNCs reveal reduced ASE thresholds of ~μJ/cm$^2$,[13] which is smaller than their counterpart for polycrystalline thin films [14] or conventional CQDs excited under similar conditions.[2] Over the past 3-4 years, a dozen of papers have been devoted to study the mechanism of optical amplification in $CsPbX_3$ (X = Br, I) PNCs.[13,15–27] Most of these works, however, still required fs excitation pulses to avoid Auger recombination, hence further investigation is needed to achieve more ambitious objectives such as lasing under CW operation or electrical pumping. Indeed, the intrinsic mechanism underlying the optical gain in PNCs remains poorly understood. It is still under debate whether single- or bi-exciton regime is realized in PNCs under threshold excitation intensities, or if free carriers are the dominant mechanism in the stimulated emission process.[28] In addition, it is not clear what is the role of self-absorption in ASE, how the photoluminescence (PL) inhomogeneous broadening can affect the ASE spectra, and what are the gain saturation mechanisms. Finally, according to the data published in different papers,[13,17,19,29] ASE spectra broad at high intensity excitation, although this behavior has not been explained yet.

In case of more traditional CQDs, it is established that the two-fold degeneracy of the band-edge states requires that, to achieve optical gain, at least some of the QDs in the sample must contain multiple excitons (that is, the average number of excitons per dot, ⟨N⟩, should be higher than 1).[1] In spite of this, there arw data that single-exciton regime of gain can be achieved in case of high-quality CQD samples possessing low optical losses [X1]. The single-exciton gain regime is the most favorable from the point of view of minimizing losses, because the non-radiative exciton-exciton recombination is impossible in this case.

In case of PNCs the two-fold degeneracy of the band-edge states is also discussed in literature,[16] and in an absolute majority of works the conclusion is drawn about the bi-exciton optical gain

mechanism in PNCs at threshold pump intensities. [15,23,30,31] However, as our analysis shows, the conclusions is made on the basis of either some features of the luminescence decay kinetics, without any spectral evidences,[23] or by the presence of a long-wavelength shift of the ASE band maximum relative to the spontaneous emission band[31] and the quadratic dependence of the integral ASE band intensities on excitation fluency.[15] In the present work, we show that the long-wavelength shift of the ASE band maximum cannot serve as the evidence of the biexciton nature of the ASE band, because it may be a result of the PL reabsorption. In addition, taking into account self-absorption losses, inhomogeneous broadening and ASE saturation in PNCs, we propose a model reproducing the ASE spectra modifications with excitation fluency. The data obtained in our low temperature experiments implemented with thin films of three different bandgap PNCs ($CsPbBr_3$, $CsPbI_3$, and $CsPbBr_{1.5}I_{1.5}$) enable us to conclude that the observed optical near-threshold gain requires less than one exciton per NC and is provided by a single-exciton mechanism.

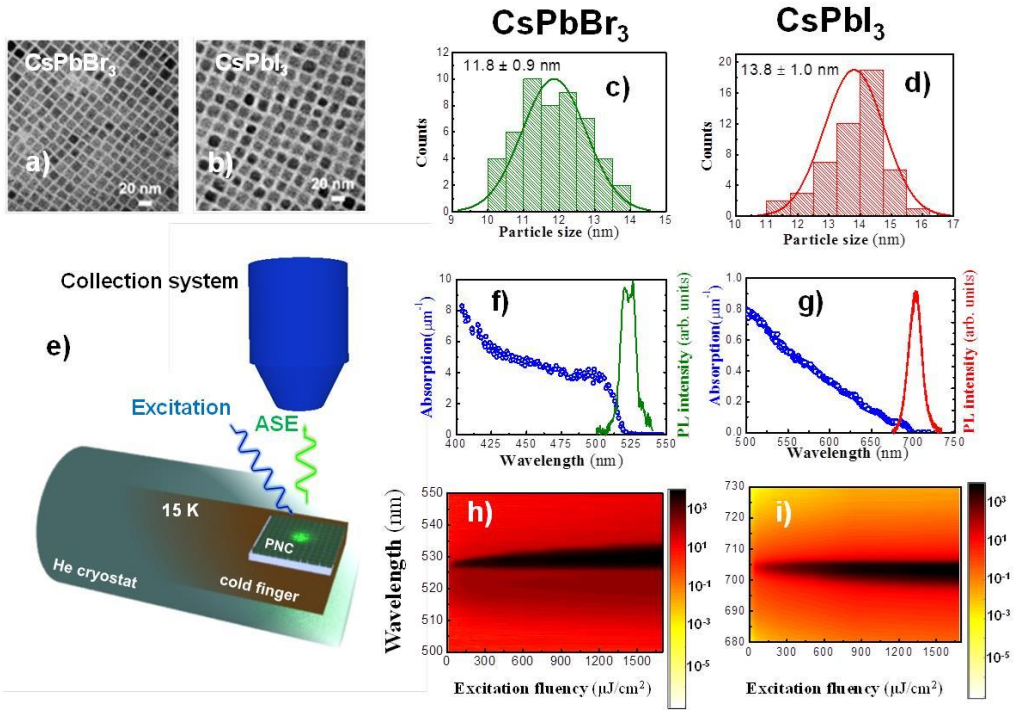


**Figure 1.** (a-b) TEM images of $CsPbBr_3$ (a) and $CsPbI_3$ (b) NCs. (c-d) Size dispersion for $CsPbBr_3$ (c) and $CsPbI_3$ (d) NCs. (e) Experimental set-up. (f-g) Absorption (blue and left axis) and PL (green/red and right axis) of $CsPbBr_3$ (f) and $CsPbI_3$(g). (h-i) 3D image of PL as a function of excitation fluency for $CsPbBr_3$ (h) and $CsPbI_3$ (i). All optical characterization was performed at 15 K.

## Experimental

$CsPbX_3$ ($X_3$=$Br_3$, $Br_{1.5}I_{1.5}$, $I_3$) were grown following the hot-injection method developed by Kovalenko et al.,[12] after the modifications detailed in the methods section. The PNCs are of the cubic shape [12] (see TEM images in Figures 1(a) and 1(b)) with an average size (L) between 11.8 nm and 13.8 with an average size dispersion of about 7 % ($CsPbBr_3$) and 13.8 nm ($CsPbI_3$),

as presented in Figures 1(c) and 1(d), respectively. Since the Bohr radius ($a_0$) of these PNS ranges between 7 ($CsPbBr_3$) and 12 nm ($CsPbI_3$) the $L/2a_0$ ratio is from 0.4 ($CsPbI_3$) and 0.8 ($CsPbBr_3$), which corresponds to the weak confinement regime.

Then, 20 nm -1 μm thick $CsPbX_3$ films were deposited on borosilicate substrates (see details of fabrication in the methods section). In order to prevent the influence of phonons or other non radiative channels in the generation of ASE, photoluminescence (PL) was studied by holding the samples on a cold finger of a closed-cycle He cryostat cooled down to 15K (see Figure 1e). In particular, absorption was characterized by measuring the sample transmittance of a xenon lamp light, and PL was measured in back scattering geometry by pumping the nanocrystals with a Q-switch Nd:YAG (1 kHz, 1 ns) laser doubled or tripled at 532 nm and 355 nm, respectively. Excitation wavelength was chosen according to the absorption band edge measured for PNCs at cryogenic temperature (see blue symbols in Figures 1f-1g): 500 nm (2.35 eV) and 685 nm (1.81 eV) for $CsPbBr_3$, and $CsPbI_3$ , respectively. The evolution of the PL spectra in PNCs films with the excitation fluency ($P_{exc}$) indicates that more than one physical mechanism influences the generation of optical gain, as illustrated in the 3D plots for 300 nm layers of $CsPbBr_3$ (Figure 1h) and $CsPbI_3$ (Figure 1i) PNCs. ASE spectra in $CsPbI_{1.5}Br_{1.5}$, films are similar to those measured with $CsPbI_3$ and are summarized in the supporting information.

**ASE in PNCs**

The behavior of $CsPbBr_3$ thin films excited at 355 nm under increasing excitation fluency $P_{exc}$ clearly presents three different regions (see Figure 2a). When $P_{exc}$< 3 μJ/cm$^2$ the PL shows a Gaussian shape centered at 522.4 nm (2.3768 eV) with a Full Width at Half Maximum (FWHM) of about 10 nm (50 meV). Similar spectral shape has been reported in literature for these PNCs at cryogenic temperature [19,32] and can be ascribed to the spontaneous emission of an exciton (marked as X in Figure 2a). When $P_{exc}$=10 μJ/cm$^2$, a narrow stimulated emission band (designated as SE in Figure 2a) appears on the long-wavelength side (526.6 nm) of the spontaneous emission, which is in agreement with the results previously reported with this material at room [13] or cryogenic[19] temperature. Then, as $P_{exc}$ is increased up to 48 μJ/cm$^2$ the SE band progressively narrows down to FWHM as low as1.37 nm (6.1 meV) and redshifts to 527.3 nm. With a further increase of $P_{exc}$ (>48 μJ/cm$^2$) the SE band continues to redshift, but its spectral width broads, so that at $P_{exc}$ ≈1.6 mJ/cm$^2$ the FWHM reaches 4.4 nm (19.4 meV) with a maximum at 530 nm (2.3409 eV). Figure 2b shows a log-log plot of the FWHM and the integrated SE ($I_{SE}$) band deconvoluted from the whole spectra (see details in the Supplementary Information) as function of $P_{exc}$ with blue and green symbols, respectively. Clearly, the dependence of $I_{SE}$ as a function of $P_{exc}$ follows the three different regions commented above. For low $P_{exc}$ (<10 μJ/cm$^2$) $I_{SE}$ obeys the linear generation of light ($I_{SE} \propto P_{exc}$) due to a spontaneous emission process. However, above a threshold of $P_{exc}$>=10 μJ/cm$^2$ $I_{SE}$ presents the superlinear dependence ($I_{SE} \propto P_{exc}^{2.3}$) characteristic of ASE, followed by a saturation for $P_{exc}$>48 μJ/cm$^2$. Indeed, there is a progressive evolution between SE and saturation that can be phenomenologically fitted (solid green line) by $\log(I_{SE})=0.65+0.95\cdot\log(P_{exc})-0.52\cdot\log^2(P_{exc})$.

Taking into account the absorption coefficient at the excitation wavelength (355 nm) shown in Figure 1f (10 $\mu m^{-1}$) and the size (L) of the PNCs, the absorption cross section ($\sigma$) can be estimated as $\sigma=\alpha \cdot L^3=1.6 \cdot 10^{-13}$ $cm^2$, which nicely agrees with the results previously published for this material. [33,34] In these conditions, the number of excitations per nanocrystal can be calculated as $<N>=P \cdot \sigma/h\nu$, and results in about 2.5 at the threshold fluency (see top axis in Figure 2b).

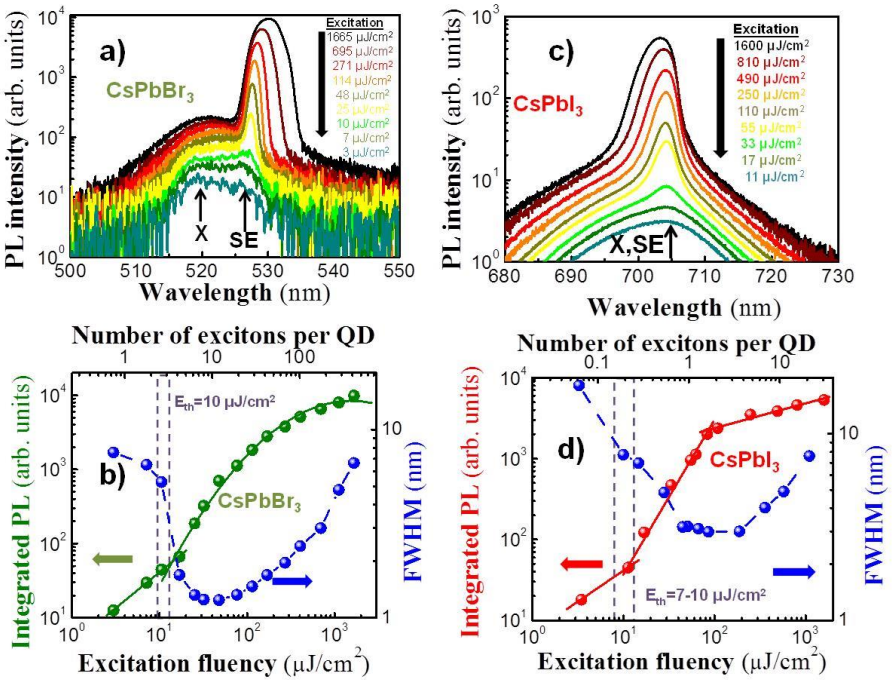


**Figure 2.** Dependence of PL of 300 nm $CsPbX_3$ layers on the excitation fluency obtained for PL spectra (a, c), integrated PL intensity (green/red symbols) and FWHM (blue symbols) (b, d) for the cases of $CsPbBr_3$ (a, b) and $CsPbI_3$ (c, d).

In case of $CsPbI_3$ (see Figure 2c) the PL excited at 532 nm presents similar $P_{exc}$ - dependence regions. For P<10 $\mu J/cm^2$ the spectrum is well described by a Gaussian shape centred at 703.6 nm (1.76 eV) with FWHM of 18.4 nm, which corresponds to the spontaneous emission band of this material at cryogenic temperature.[32] When $P_{exc}$ >10 $\mu J/cm^2$ the spectra start narrowing down to 3 nm at $P_{exc}$<78 $\mu J/cm^2$; and, with a further increase of $P_{exc}$ the spectra progressively broads up to 7.7 nm for $P_{exc}$ =1.6 $mJ/cm^2$. Figure 2d presents the evolution of the FWHM and integrated intensity with $P_{exc}$ with blue and red symbols, respectively. Again, this log-log plot clearly distinguishes the three regions commented above: spontaneous emission ($I_{SE} \propto P_{exc}$) for $P_{exc}$<10 $\mu J/cm^2$ , stimulated emission ($I_{SE} \propto P_{exc}^{1.8}$) above a threshold of $P_{exc}$ =10 $\mu J/cm^2$, and saturation ($I_{SE} \propto P_{exc}^{0.3}$) for $P_{exc}$>78$\mu J/cm^2$. There are, however, some interesting differences compared with the behaviour presented by $CsPbBr_3$ PNCs thin films: (i) SE band is centered at the maximum of the spontaneous PL, hence this band does not redshift with $P_{exc}$; (ii) the border between SE and saturation is sharper here; (iii) in agreement with previous publications,[16] absorption coefficient (0.5 $\mu m^{-1}$) is smaller than that measured for $CsPbBr_3$ (see

Figure 1g), and with it <N> is at the level of 0.2-0.3 at the threshold excitation intensity (see Figure 1d).

**Single exciton gain and self absorption**

As analysis of literature data on optical gain in perovskite nanocrystals shows, it is very inviting to say that the observed stimulated emission band is due to the so-called biexcitonic emission (biexciton - exciton transition).[27] Indeed, it is commonly accepted for semiconductor quantum dots (QDs) such as CdSe etc., that the optical gain in these nanostructures may be only due to the biexciton-exciton transition that is a result of double degeneracy of the electronic states. [3,7] The bi-excitonic SE band usually appears at energies ($E_{XX}$) which are lower than the one-exciton emission energy $E_X$. The energy difference $E_{bXX}=E_X-E_{XX}$ is the so-called "the biexciton binding energy". In our results with $CsPbBr_3$ layers the energy difference between the spontaneous emission and SE band maxim is 20.8 meV that well correlates with results of other works.[16,23] A reliable proof of the biexciton nature of the SE band is also considered to be the quadratic dependence of the integral SE band intensity on the excitation density at the initial stage of its occurrence. [7,15] In fact, we have such a dependence for both $CsPbBr_3$ and $CsPbI_3$ PNCs samples (Figure 2b and 2d). Therefore, from the point of view of typical proofs we found in literature, we have experimental data, which are in line with the idea about biexcitonic origin of the SE band.

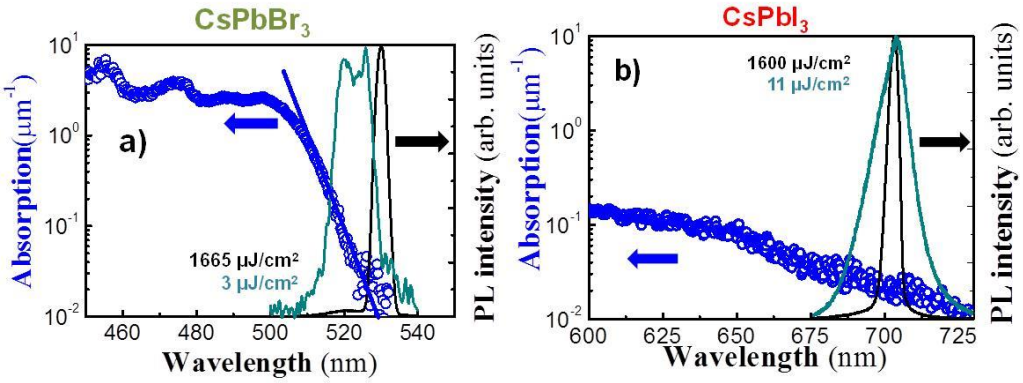


**Figure 3.** Absorption in log scale (blue symbols) and PL spectra at 10 μJ/cm$^2$ (cyan) and 1600 mJ/cm$^2$measured for $CsPbBr_3$ (a) and $CsPbI_3$ (b) layers of 300 nm thickness.

However, a number of observations leads us to doubt the validity of such a conclusion. First is that, in case of $CsPbI_3$ NCs, the SE band appears exactly at the maximum of the single-excitonic spontaneous emission band (Figure 2c). It implies that the biexciton binding energy $E_{bXX}=E_X-E_{XX}=0$ that is inconsistent with the biexciton SE emission model. Second, the $I_{SE} \propto P_{exc}^2$ dependence found in the log-log curves presented in Figures 2c and 2d is correlated with the narrowing of the spectra; hence it must be definitively ascribed to an ASE mechanism, where it is well-known that the intensity of light follows a nonlinear dependence with the excitation fluency.[35] – VC: I do not understand Finally, the overlap of the band edge absorption spectra with the PL emission suggests that the value of the PL vs absorption edge redshift is influenced by self-absorption effects (Figure 3). In the case of $CsPbBr_3$ (Figure 3a) the absorption exhibits a

sharp Urbach tail (blue symbols) overlapping the spontaneously emitted PL (cyan line), in agreement with the results published elsewhere. [16,33,36] Due to this, PL experiences an asymmetric attenuation ($10^{-2}$ and $10^{-1}$ $\mu m^{-1}$ for the shortest and longest wavelength, respectively), and the ASE at the highest excitation (black line) is located at the region with a negligible absorption (>530 nm). On the other hands, according to previous publications, [16] $CsPbI_3$ layers (Figure 3b) demonstrate lower ($<10^{-2}$ $\mu m^{-1}$) absorption intensity (blue symbols) in the PL band (cyan line). Consequently, $E_X$-$E_{SE}$=0 in this material and the ASE spectra (black line) does not exhibit a redshift with excitation intensity.

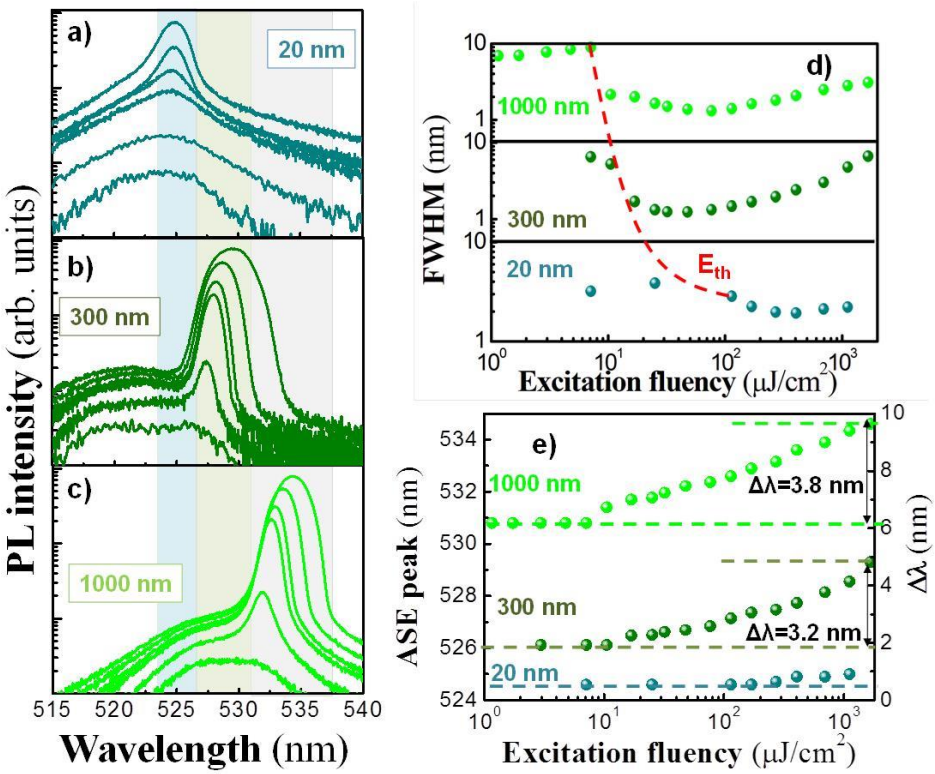


**Figure 4.** (a-c) PL spectra of $CsPbBr_3$ layers as a function of the excitation fluency measured for the layer thicknesses of 20 nm (a), 300 nm (b), and 1000 nm (c). (d) FWHM as a function of the excitation fluency for the three different thickness. Threshold decreases with excitation fluency. (e) Shift of ASE peak as a function of the excitation fluency and thickness of the sample.

Indeed, our SE spectra measurements for $CsPbBr_3$ NCs samples of different thicknesses (Figure 4a-4c) unambiguously demonstrate that the difference $E_X$-$E_{SE}$ decreases with the sample thickness. Of course, this decrease is certainly inconsistent with the biexciton SE emission model from one side and evidences in favour of self-absorption effect on the other hand. Indeed, metal halide perovskites (MHPs) are known to have strongly overlapping absorption and PL spectra that results in strong PL self-absorption.[37] Especially favourable for reabsorption is the geometry of thin films, where the high confinement of light can enhance the intrinsic absorption or gain effects. [38] The effect results in a redshift of the PL band maximum, [39] and this is even more

dramatically the ASE, [38] because it is very sensitive to the optical losses. Here, we consider some kind of isotropic propagation through the PNC film, where a thicker layer results in a longer path for the emitted photons (see the model below for further details). Consequently, the expected reduction of ASE threshold for thicker layers (see Figure 4d) correlates with the red shift of the ASE peak (see Figure 4e).

Therefore, our data on the SE spectra dependence on the sample thickness (Figure 4) unambiguously evidence that value of $E_X$-$E_{SE}$ depends on the sample thickness and visually tends to zero with the thickness decrease (Figure 4e). The logical explanation of the Figure 4 data is that the initial shift (about 4 nm) between the just emerging SE band and the spontaneous emission (mono-excitonic) band is due to PL self-absorption, which introduces losses in the region where PL and absorption overlaps. Thus, such a full-optical approach well explains our observations and does not require an introduction of biexcitonic emission at near-threshold excitation intensities and enables one to account for the observed SE by one-exciton mechanism. As is well established for conventional semiconductor QDs, such single-exciton SE is impossible for neutral (uncharged) QDs because of double-degenerate origin of their quantum states, but possible for charged ones (trions etc.).[16] We believe that there are two possible explanations of the observed one-exciton gain in case of MHPs: i) photocharging of NCs due to well known for MHPs non-quenching trapping of one of carriers by shallow traps [X2], or ii) inapplicability of the state filling model for MHP NCs.

Now we have to discuss the question of why we continue to observe a single-exciton SE band at excitation densities that provide up to 10 or more excitations per nanocrystal, although the formally calculated excitation density significantly exceeds the Mott density at which excitons should dissociate ($10^{17}$ $cm^{-3}$ at 15 K, see calculations in Supporting information)? We believe that there are several reasons for this. First, the nanosecond excitation we use is a quasi-stationary mode in which the duration of the excitation pulse is longer or comparable to the lifetime of the excitations. Due to this, the excitons interact with each other (form biexcitons, annihilate) already during the excitation pulse that results in abrupt shortening of the PL decay kinetics (see Figure S2). Therefore, the formal use of the average number of excitations per pulse per nanoparticle poorly describes the situation: in fact, in the ensemble at any time there should be only single-excitons and some quantity of biexcitons. However, biexcitons are not visible spectrally at excitation densities up to 75 $\mu J/cm^2$; under more intense excitation, however, they can take part in the formation of the broadened SE band. One more reason why biexcitons (and possibly stimulated emission due to charge recombination in electron-hole plasma (EHP)) is not visible is that we detect integral emission when mainly long-lived species contribute to the PL profile, whereas contribution of short-lived species (emission from EHP and/or biexcitons) can be neglected. Only high temporal resolution spectrally resolved measurements can clarify the situation and give an idea about short-lived participants of the recombination processes [X3].

**SE band broadening**

One more important question to be answered is a reason of the SE band broadening which starts when excitation fluency exceeds 100 $\mu J/cm^2$ (Figure 2a-2c). We believe that,

regardless of the nature of the SE band, a change in its shape can be the result of two effects: inhomogeneous broadening of the luminescence contour (see Figures 1f-1g), which correlated with the size dispersion, [40,41] (see Figures 1c-1d) and the gain saturation effect,[35,41] which is most pronounced for the most intensely luminescent nanocrystals. Such saturation occurs in optical amplifiers [35] due to the lack of empty excited states along the optical path; and in the case of semiconductor nanocrystals it starts at the centre of the PL because the QDs with emission at this wavelength have the highest occupation probability. In this way, the higher the luminescence intensity, the earlier the saturation is achieved. Therefore, when the gain saturation region is reached the spectral edges of the CE band grow in intensity faster than the central part of the band, as observed in Figures 2a and 2c.

**Modelling**

Taking into account the physical and optical mechanisms discussed in the previous section (exciton gain, self absorption, gain saturation and inhomogeneous broadening) we developed a model whose results are presented in Figure 5. For this purpose, we consider that the excitation beam homogeneously illuminates a diameter of 100 μm, and it is being attenuated while the pump beam is traversing the sample:

$$P_{exc} = P_0 e^{-\alpha_{355}(L-z)} \quad (1)$$

The number of electron hole-pairs ($N_{eh}$) at each propagation step is given by:

$$N_{eh}(z) = \frac{\alpha_{355} \cdot P_{exc}(z)}{h\nu} \quad (2)$$

where α is the absorpiton coefficient? at the exciation wavelength (355 nm and 532 nm). Then, PL is generated isotropically through this cylinder,

$$P_{PL(z_i,\lambda)} = QY(P_{exc}) \cdot N_{eh}(zi) \cdot PL(\lambda) \quad (3)$$

where Quantum Yield (QY) is defined as the ratio of the integral PL intensity to the excitation intensity and decreases continuously with increasing excitation energy density (see Supporting Information) and PL is the spectral shape of the spontaneous emission assumed as a Gaussian distribution centered at 520 nm (2.37 eV) with a FWHM of 10 nm (45.5 meV):

$$PL(E) = \frac{PL_0}{w_{in} \cdot \sqrt{\pi/2}} \cdot e^{-2\frac{(E-E_0)^2}{w_{in}^2}} \quad (4)$$

Here, if one considers an inhomogeneous broadening of the PL in the QDs, the emission of a single nanoparticle is given by a Lorentzian distribution (w=2 meV and 130 QDs with a step of 1 meV are considered): [41]

$$L(E_k) = PL(E) \cdot \frac{1}{4 \cdot (E-E_k)^2 + w^2} \quad (5)$$

where the sum of the emission of all nanoparticles gives PL(E). In this way, each QD will emit light at each propagation step according to the following rate equations:

$$\frac{dN}{dt} = G - \sum_k \frac{N}{\tau} \cdot \frac{1}{w_{in} \cdot \sqrt{\pi/2}} \cdot e^{-2\frac{(E-E_0)^2}{w_{in}^2}} \quad (6)$$

$$\frac{dn_k}{dt} = N_k - \frac{n_k}{\tau_r} - \frac{n_k^2}{\tau_{xx}} - (n_k - N_0)\cdot\sigma\cdot\frac{S}{h\cdot\vartheta} \quad (7)$$

$$N_k = \frac{N}{\tau}\cdot\frac{1}{w_{in}\cdot\sqrt{\pi/2}}\cdot e^{-2\frac{(E_k-E_0)^2}{w_{in}^2}} \quad (8)$$

where G is the number of electron-hole pairs per pulse, N the number of carriers in excited states, $n_k$ is the number of excitons with the energy k, $\tau_r$ the radiative recombination time, $\tau_{xx}$ the time of formation of biexcitons, $N_0$ the threshold of stimulated emission, σ the emission cross section, S the signal fluency and hν the photon energy of the signal. Here, a saturation condition is introduced to include that the number of PNCs with emission at a given wavelength can not overcome the maximum density of nanocrystals (inverse volume correlated but the inhomogeneous size??). Finally, the evolution of the signal along the path is obtained by solving the propagation equation with a Runge-Kutta algorithm:

$$\frac{dS}{dz} = (g-\alpha)\cdot S + N_{eh}\cdot PL\cdot\tau_r\cdot\delta \quad (9)$$

where PL is the shape of the spontaneous emission, δ a fitting parameter and g the gain given by:

$$g_k = \sigma\cdot n_k\cdot S_{norm} \quad (10)$$

where $S_{norm}$ is the shape of the S in the previous step. The introduction of the wavelength dependent losses clearly results in the ASE spectra redshift (Figure 5b), while in case of α=0 ASE does not demonstrate any redshift (Figure 5c). In both cases, the model reproduces the gain saturation mechanism proposed here and the consequent broadening of the ASE band due to the generation of stimulated emission at the tails of the PL band when the layers are pumped under high excitation fluencies (Figures 5b-5c).

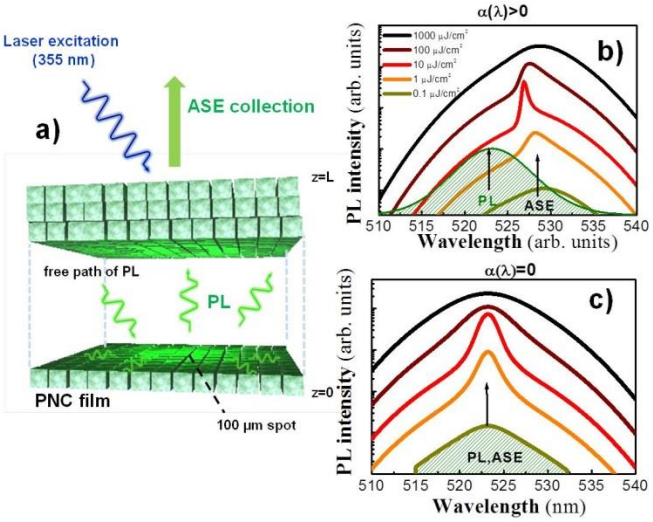


**Figure 5** Modelling of the SE band broadening due to gain saturation effect: (a) schematic presentation of the experiment geometry; (b) results when self-absorption is inckuded in calculations; (c) results with negligible reabsorption effect.

## Conclusions

In summary, we stablish the role of the different species (exciton, biexciton, free carriers) and physical mechanisms (reabsorption effect, inhomogeneous broadening of the PL band, gain saturation) in the generation of optical gain in PNCs. Although biexcitonic emission is usually the preferred mechanism to explain the stimulated emission in these nanoparticles, our experimental data evidence that ASE is produced by a single exciton. In particular, the comparison of the ASE spectra in $CsPbBr_3$ with different thicknesses reveals that the experimental redshift observed for ASE depends on the thickness, which is incompatible with the biexcitonic emission and suggests the influence of reabsorption effects. In addition, we establish the influence of the inhomogeneous size of the PNCs, which results in the gain saturation at the most intensively luminescent nanocrystals and the consequent broadening of the ASE spectra under high excitation fluencies. All physical and optical mechanisms are introduced in a rate equation model able to reproduce the experimental ASE spectra. These results help for a better understanding of the generation of light in PNCs, and the future development of ASE under continuous wave (or electrical) operation.

## Methods

*Synthesis of Colloidal solution*. $CsPbX_3$ NPs were synthetized following the hot-injection method described by Kovalenko and coworkers, with some modifications.[12] All the reactants were used as received without additional purification process. Briefly, a Cs-oleate solution was prepared by mixing 0.41 g $Cs_2CO_3$ (Sigma-Aldrich, 99.9 %), 1.25 mL of oleic acid (OA, Sigma Aldrich, 90 %) and 20 mL of 1-octadecene (1-ODE, Sigma-Aldrich, 90 %) into a 50 mL-three neck flask at 120 °C under vacuum for 1 h, keeping a constant stirring. Then, the mixture was $N_2$-purged and heated at 150°C until the $Cs_2CO_3$ was completely dissolved. The solution was stored under $N_2$, keeping the temperature at 100 °C to prevent the Cs-oleate oxidation.

For the synthesis of $CsPbBr_3$, $CsPbI_3$ and $CsPbBr_{1.5}I_{1.5}$ NPs, 0.69 g $PbBr_2$ (ABCR, 99.999 %), 0.87 g $PbI_2$ (TCI, 99.99 %) or the corresponding $PbBr_2/PbI_2$ mixture, were mixed with 50 mL of 1-ODE into a 100 mL-three neck flask. The mixture was heated at 120 °C under vacuum for 1 h, keeping a constant stirring. Then, 5 mL of both OA and oleylamine (OLA, Sigma-Aldrich, 98 %) were separately added to the flask under $N_2$, and rapidly heated to reach 170 °C, injecting quickly 4 mL of Cs-oleate solution. Lastly, the flask was immersed into a bath ice for 5 s to quench the reaction mixture.

For the isolation of PNPs, the colloidal solutions were centrifugated at 4700 rpm for 10 min. The NPs pellets were separated after discarding the supernatant and redispersed in hexane to prepare a concentration of 50 mg $mL^{-1}$.

*Sample preparation*. PNPs were deposited on a commercial borosilicate substrate by using a commercial Doctor Blade applicator (Elcometer 4340) and post-baking at 100 ºC for 1 minute. These steps have been sequentially repeated until the film of PNPs reached the desired thickness

(20 nm-1 μm). Prior to the deposition substrates were carefully cleaned with acetone, ethanol and isopropanol during 10 minutes in an ultrasound bath.

*Absorption and photoluminescence*. A commercial NanoCalc-2000 reflectometer (Mikropack) was used to measure absorption spectra in $CsPbX_3$ films deposited on borosilicate substrates.

*Low temperature PL and TRPL*. Samples were held in a cold finger of a closed-cycle He cryostat, which can be cooled down to 10K. PL was measured by using a Q-switch Nd:Yag (1 kHz, 1 ns) laser doubled or tripled at 532 nm and 355 nm (CRYLAS 6FTSS355- Q4-S), respectively. The PL signal was dispersed by a double 0.3 m focal length grating spectrograph and detected with a back illuminated Si CCD. Time-resolved PL was carried out by using the same pumping laser, but analyzing the PL with a Hamamatsu C5658−3769 avalanche photodetector connected to a BOXCARDPCS-150 electronics from Becker and Hickl GmbH. PL under femtosecond operation was carried out by using PL a Ti:sapphire mode locked laser at a wavelength of 405 nm doubled by a BBO crystal. In this case, Time-resolved PL have been carried out with the Ti:sapphire laser in pulsed mode operation (pulse width 2 ps and 76 MHz of repetition rate) at the same wavelength. In this case, the emitted signal is collected by a Si avalanche photodiode connected to a time correlated single photon counting electronics.

**Acknowledgements**

Financial support by Spanish MINECO through project nº TEC2017-86102-C2-1-R and the European Research Council (ERC) via Consolidator Grant (724424 - No-LIMIT) are gratefully acknowledged. J.N. Arenas acknowledges MINECO for the support through FPI Fellowship Program (XXXX).

**References**

(1) Pietryga, J. M.; Park, Y. S.; Lim, J.; Fidler, A. F.; Bae, W. K.; Brovelli, S.; Klimov, V. I. Spectroscopic and Device Aspects of Nanocrystal Quantum Dots. *Chem. Rev.* **2016**, *116* (18), 10513–10622.

(2) Suárez Alvarez, I. Active Photonic Devices Based on Colloidal Semiconductor Nanocrystals and Organometallic Halide Perovskites. *Eur. Phys. J. Appl. Phys.* **2016**, *75* (3), 30001.

(3) Klimov, V. I.; Mikhailovsky, A. A.; Xu, S.; Malko, A.; Hollinngsworth, J. A.; Leatherdale, C. A.; Eisler, H. J.; Bawendi, M. G. Optical Gain and Stimulated Emission in Nanocrystal Quantum Dots. *Science (80-. ).* **2000**, *290* (5490), 314–317.

(4) Fan, F.; Voznyy, O.; Sabatini, R. P.; Bicanic, K. T.; Adachi, M. M.; McBride, J. R.; Reid, K. R.; Park, Y. S.; Li, X.; Jain, A.; et al. Continuous-Wave Lasing in Colloidal Quantum Dot Solids Enabled by Facet-Selective Epitaxy. *Nature* **2017**, *544* (7648), 75–79.

(5) Lim, J.; Park, Y. S.; Klimov, V. I. Optical Gain in Colloidal Quantum Dots Achieved with Direct-Current Electrical Pumping. *Nat. Mater.* **2018**, *17* (1), 42–48.

(6) Dang, C.; Lee, J.; Breen, C.; Steckel, J. S.; Coe-Sullivan, S.; Nurmikko, A. Red, Green

and Blue Lasing Enabled by Single-Exciton Gain in Colloidal Quantum Dot Films. *Nat. Nanotechnol.* **2012**, *7* (5), 335–339.

(7) Klimov, V. I.; Ivanov, S. A.; Nanda, J.; Achermann, M.; Bezel, I.; McGuire, J. A.; Piryatinski, A. Single-Exciton Optical Gain in Semiconductor Nanocrystals. *Nature* **2007**, *447* (7143), 441–446.

(8) Garcia-Santamaria, F.; Chen, Y.; Vela, J.; Schaller, R. D.; Hollingsworth, J. A.; Klimov, V. I. Suppressed Auger Recombination in "Giant" Nanocrystals Boosts Optical Gain Performance. *Nano Lett.* **2009**, *9* (10), 3482–3488.

(9) Woo, C.; CJ Wang; Guyot-Sionnest, P.; Wehrenberg, B. Light Emission and Amplification in Charged CdSe Quantum Dots. *J. Phys. Chem. B* **2004**, *108* (26), 9027–9031.

(10) Akkerman, Q. A.; Rainò, G.; Kovalenko, M. V.; Manna, L. Genesis, Challenges and Opportunities for Colloidal Lead Halide Perovskite Nanocrystals. *Nat. Mater.* **2018**, *17*, 394–405.

(11) Saouma, F. O.; Park, D. Y.; Kim, S. H.; Jeong, M. S.; Jang, J. I. Multiphoton Absorption Coefficients of Organic–Inorganic Lead Halide Perovskites CH 3 NH 3 PbX 3 (X = Cl, Br, I) Single Crystals. *Chem. Mater.* **2017**, *29*, 6876–6882.

(12) Protesescu, L.; Yakunin, S.; Bodnarchuk, M. I.; Krieg, F.; Caputo, R.; Hendon, C. H.; Yang, R. X.; Walsh, A.; Kovalenko, M. V. Nanocrystals of Cesium Lead Halide Perovskites (CsPbX3 , X = Cl, Br, and I): Novel Optoelectronic Materials Showing Bright Emission with Wide Color Gamut. *Nano Lett.* **2015**, *15* (6), 3692–3696.

(13) Yakunin, S.; Protesescu, L.; Krieg, F.; Bodnarchuk, M. I.; Nedelcu, G.; Humer, M.; De Luca, G.; Fiebig, M.; Heiss, W.; Kovalenko, M. V. Low-Threshold Amplified Spontaneous Emission and Lasing from Colloidal Nanocrystals of Caesium Lead Halide Perovskites. *Nat. Commun.* **2015**, *6*, 8056.

(14) Xing, G.; Mathews, N.; Lim, S. S.; Yantara, N.; Liu, X.; Sabba, D.; Grätzel, M.; Mhaisalkar, S.; Sum, T. C. Low-Temperature Solution-Processed Wavelength-Tunable Perovskites for Lasing. *Nat. Mater.* **2014**, *13* (5), 476–480.

(15) Wang, Y.; Li, X.; Song, J.; Xiao, L.; Zeng, H.; Sun, H. All-Inorganic Colloidal Perovskite Quantum Dots: A New Class of Lasing Materials with Favorable Characteristics. *Adv. Mater.* **2015**, *27* (44), 7101–7108. - see Ref. 29

(16) Makarov, N. S.; Guo, S.; Isaienko, O.; Liu, W.; Robel, I.; Klimov, V. I. Spectral and Dynamical Properties of Single Excitons, Biexcitons, and Trions in Cesium-Lead-Halide Perovskite Quantum Dots. *Nano Lett.* **2016**, *16*, 2349–2362.

(17) Chen, S.; Nurmikko, A. Stable Green Perovskite Vertical-Cavity Surface-Emitting Lasers on Rigid and Flexible Substrates. *ACS Photonics* **2017**, *4* (10), 2486–2494.

(18) Wang, Y.; Li, X.; Nalla, V.; Zeng, H.; Sun, H. Solution-Processed Low Threshold Vertical Cavity Surface Emitting Lasers from All-Inorganic Perovskite Nanocrystals. *Adv. Funct. Mater.* **2017**, *27* (13), 1605088.

(19) Balena, A.; Perulli, A.; Fernandez, M.; De Giorgi, M. L.; Nedelcu, G.; Kovalenko, M. V.; Anni, M. Temperature Dependence of the Amplified Spontaneous Emission from CsPbBr 3 Nanocrystal Thin Films. *J. Phys. Chem. C* **2018**, acs.jpcc.8b01419.

(20) Pan, J.; Sarmah, S. P.; Murali, B.; Dursun, I.; Peng, W.; Parida, M. R.; Liu, J.; Sinatra, L.; Alyami, N.; Zhao, C.; et al. Air-Stable Surface-Passivated Perovskite Quantum Dots for Ultra-Robust, Single- and Two-Photon-Induced Amplified Spontaneous Emission. *J. Phys. Chem. Lett.* **2015**, *6* (24), 5027–5033.

(21) Tong, Y.; Bladt, E.; Aygüler, M. F.; Manzi, A.; Milowska, K. Z.; Hintermayr, V. A.; Docampo, P.; Bals, S.; Urban, A. S.; Polavarapu, L.; et al. Highly Luminescent Cesium Lead Halide Perovskite Nanocrystals with Tunable Composition and Thickness by Ultrasonication. *Angew. Chemie - Int. Ed.* **2016**, *55* (44), 13887–13892.

(22) Xu, Y.; Chen, Q.; Zhang, C.; Wang, R.; Wu, H.; Zhang, X.; Xing, G.; Yu, W. W.; Wang, X.; Zhang, Y.; et al. Two-Photon-Pumped Perovskite Semiconductor Nanocrystal Lasers. *J. Am. Chem. Soc.* **2016**, *138* (11), 3761–3768.

(23) Castañeda, J. A.; Nagamine, G.; Yassitepe, E.; Bonato, L. G.; Voznyy, O.; Hoogland, S.; Nogueira, A. F.; Sargent, E. H.; Brito Cruz, C. H.; Padilha, L. A. Efficient Biexciton Interaction in Perovskite Quantum Dots Under Weak and Strong Confinement. *ACS Nano* **2016**, *10* (9), 8603–8609.

(24) Yumoto, G.; Tahara, H.; Kawawaki, T.; Saruyama, M.; Sato, R.; Teranishi, T.; Kanemitsu, Y. Hot Biexciton Effect on Optical Gain in CsPbI3 Perovskite Nanocrystals. *J. Phys. Chem. Lett.* **2018**, *9* (9), 2222–2228.

(25) Nagamine, G.; Rocha, J. O.; Bonato, L. G.; Nogueira, A. F.; Zaharieva, Z.; Watt, A. A. R.; De Brito Cruz, C. H.; Padilha, L. A. Two-Photon Absorption and Two-Photon-Induced Gain in Perovskite Quantum Dots. *J. Phys. Chem. Lett.* **2018**, *9* (12), 3478–3484.

(26) Wang, Y.; Zhi, M.; Chang, Y. Q.; Zhang, J. P.; Chan, Y. Stable, Ultralow Threshold Amplified Spontaneous Emission from CsPbBr3 Nanoparticles Exhibiting Trion Gain. *Nano Lett.* **2018**, *18* (8), 4976–4984.

(27) Zhao, W.; Qin, Z.; Zhang, C.; Wang, G.; Huang, X.; Li, B.; Dai, X.; Xiao, M. Optical Gain from Biexcitons in CsPbBr 3 Nanocrystals Revealed by Two-Dimensional Electronic Spectroscopy. *J. Phys. Chem. Lett.* **2019**, *10* (6), 1251–1258.

(28) Geiregat, P.; Maes, J.; Chen, K.; Drijvers, E.; De Roo, J.; Hodgkiss, J. M.; Hens, Z. Using Bulk-like Nanocrystals to Probe Intrinsic Optical Gain Characteristics of Inorganic Lead Halide Perovskites. *ACS Nano* **2018**, *12*, 10178–10188.

(29) Wang, Y.; Li, X.; Song, J.; Xiao, L.; Zeng, H.; Sun, H. All-Inorganic Colloidal Perovskite Quantum Dots: A New Class of Lasing Materials with Favorable Characteristics. *Adv. Mater.* **2015**, n/a-n/a. - see Ref. 15

(30) Yumoto, G.; Tahara, H.; Kawawaki, T.; Saruyama, M.; Sato, R.; Teranishi, T.; Kanemitsu, Y. Hot Biexciton Effect on Optical Gain in CsPbI 3 Perovskite Nanocrystals. *J. Phys. Chem. Lett.* **2018**.

(31) Zhao, W.; Qin, Z.; Zhang, C.; Wang, G.; Huang, X.; Li, B.; Dai, X.; Xiao, M. Optical

Gain from Biexcitons in CsPbBr 3 Nanocrystals Revealed by Two-Dimensional Electronic Spectroscopy. *J. Phys. Chem. Lett.* **2019**, 1251–1258.

(32) Diroll, B. T.; Zhou, H.; Schaller, R. D. Low-Temperature Absorption, Photoluminescence, and Lifetime of CsPbX3 (X = Cl, Br, I) Nanocrystals. *Adv. Funct. Mater.* **2018**, *28* (30), 1800945.

(33) Chen, J.; Žídek, K.; Chábera, P.; Liu, D.; Cheng, P.; Nuuttila, L.; Al-Marri, M. J.; Lehtivuori, H.; Messing, M. E.; Han, K.; et al. Size- and Wavelength-Dependent Two-Photon Absorption Cross-Section of CsPbBr 3 Perovskite Quantum Dots. *J. Phys. Chem. Lett.* **2017**, *8* (10), 2316–2321.

(34) Maes, J.; Balcaen, L.; Drijvers, E.; Zhao, Q.; De Roo, J.; Vantomme, A.; Vanhaecke, F.; Geiregat, P.; Hens, Z. Light Absorption Coefficient of CsPbBr3 Perovskite Nanocrystals. *J. Phys. Chem. Lett.* **2018**, *9* (11), 3093–3097.

(35) Rosencher, E.; Vinter, B. *Optoelectronics*; Press, C. U., Ed.; 2002.

(36) She, C.; Fedin, I.; Dolzhnikov, D. S.; Demortière, A.; Schaller, R. D.; Pelton, M.; Talapin, D. V. Low-Threshold Stimulated Emission Using Colloidal Quantum Wells. *Nano Lett.* **2014**, *14* (5), 2772–2777.

(37) Stranks, S. D.; Hoye, R. L. Z.; Di, D.; Friend, R. H.; Deschler, F. The Physics of Light Emission in Halide Perovskite Devices. *Adv. Mater.* **2018**, *1803336*, 1–11.

(38) Suárez, I.; Juárez-Pérez, E. J.; Bisquert, J.; Mora-Seró, I.; Martínez-Pastor, J. P. Polymer/Perovskite Amplifying Waveguides for Active Hybrid Silicon Photonics. *Adv. Mater.* **2015**, *27* (40), 6157–6162.

(39) Gordillo, H.; Suarez, I.; Abargues, R.; Rodriguez-Canto, P.; Martinez-Pastor, J. P. Color Tuning and White Light by Dispersing CdSe, CdTe, and CdS in PMMA Nanocomposite Waveguides. *IEEE Photonics J.* **2013**, *5* (2), 2201412–2201412.

(40) Tan, C. L.; Wang, Y.; Djie, H. S.; Ooi, B. S. The Role of Optical Gain Broadening in the Ultrabroadband InGaAs/GaAs Interband Quantum-Dot Laser. *Comput. Mater. Sci.* **2008**, *44* (1), 167–173.

(41) Kim, J.; Meuer, C.; Bimberg, D.; Eisenstein, G. Effect of Inhomogeneous Broadening on Gain and Phase Recovery of Quantum-Dot Semiconductor Optical Amplifiers. *IEEE J. Quantum Electron.* **2010**, *46 SRC*- (11), 1670–1680.

X1. Dang, C.; Lee, J.; Breen, C.; Steckel, J. S.; Coe-Sullivan, S.; Nurmikko, A. Red, green and blue lasing enabled by single-exciton gain in colloidal quantum dot films. *Nat. Nanotechnol.* **2012**, *7*, 335-339.

X2. Chirvony, V. S.; González-Carrero, S.; Suárez, I.; Galian, R. E.; Sessolo, M.; Bolink, H. J.; Martínez-Pastor, J. P.; Pérez-Prieto, J. Delayed luminescence in lead halide perovskite nanocrystals. *J. Phys. Chem. C* **2017**, *121*, 13381-13390.

X3. Nagai, T.; Yamamoto, A.; Kanemitsu, Y. Photoluminescence dynamics of GaN under

intense band-to-band and exciton resonant excitation. *Phys. Rev. B* **2005,** *71*, 121201(R).